Supporting Information

Chislock et al. 10.1073/pnas.1304188110

SI Materials and Methods

Cell Culture. Primary human umbilical vein endothelial cells (HUVECs) were obtained from Lonza/Clonetics and used between passages 2 and 6. Human microvascular endothelial cells (HMVECs) immortalized with telomerase reverse transcriptase (hTERT) were provided by Xiao-Fan Wang (Duke University) (1). Endothelial cells were routinely cultured in endothelial growth medium-2 microvascular (EGM-2MV).

Endothelial Cell Viability/Apoptosis Assays. Primary HUVECs (5×10^3 cells per well in 96-well plates) were cultured in serum-free medium [endothelial basal medium-2 (EBM-2) with 0.2% BSA] for 24–48 h. Some cells were supplemented with either VEGF (100 ng/mL) or basic FGF (bFGF; 10 ng/mL). Abl kinases were inhibited by treatment with imatinib (10 μM). Cell viability in triplicate samples was assessed using CellTiter assay (Promega). In separate experiments, cells were lysed after 24-h serum starvation and cleaved caspase-3 levels were examined by Western blotting. HUVECs expressing control microRNA (miRNA) or *Abl*/*Arg* miRNAs were serum starved for 24 h (96 h post miRNA infection). Caspase activity was assessed in triplicate samples using the Caspase-3/7-Glo assay (Promega) and normalized to total cell number. For Angpt1-mediated survival experiments, 200 ng/mL Angpt1 (C-terminal 6-His tag) was preincubated with 20 μg/mL anti-polyhistidine cross-linking antibody for 1 h at 37 °C in serum-free medium before treatment of HUVECs.

Inhibitors and Reagents. Imatinib (Gleevec/STI571) was a generous gift from Novartis. Recombinant human vascular endothelial growth factor (VEGF-A-165), recombinant human angiopoietin-1 (C-terminal 6-His tag), and anti-polyhistidine cross-linking antibody were purchased from R&D Systems. Recombinant human bFGF was purchased from Invitrogen.

Antibodies. Antibodies used for immunohistochemistry included CD31 (BD Biosciences), von Willebrand factor (vWF) and fibrin/fibrinogen (Dako), CD41 (eBioscience), α-smooth muscle actin (Sigma), and cleaved caspase-3 (Cell Signaling). Antibodies used for Western blotting included cleaved caspase-3, phospho-CrkL (Y207), VEGF receptor 2 (VEGFR2, anti-human), phospho-Akt(S473), Akt, and phospho-Erk(T202/Y204) from Cell Signaling; β-tubulin from Sigma–Aldrich; Arg (9H5), Angpt2, VEGFR2 (anti-mouse, Flk-1), Erk, lamin B, and CrkL from Santa Cruz; anti-Abl (clone 8E9) from BD Biosciences; and phospho-Tie2(Y992) (tyrosine kinase with immunoglobulin and epidermal growth factor homology domains-2) from R&D Systems. Mouse monoclonal antibody (Ab33) against Tie2 was a gift from Christopher Kontos (Duke University) (2).

Mouse Endothelial Cell Isolation, Flow Cytometric Analysis, and Characterization of Abl Inactivation. E13.5 embryos (wild-type or Abl^{ECKO}; $Arg^{-/-}$) were disrupted by trituration and digested in 1 mg/mL collagenase A solution (in low-glucose DMEM, supplemented with 1% penicillin–streptomycin, gentamicin, and 25 μg/mL DNase I) for 45 min at 37 °C. The cell suspension was then disrupted by passage (20 times) through a syringe with an attached 14-gauge cannula and filtered through a 70-μm cell strainer, followed by red blood cell lysis. Cells were incubated first for 15 min on ice with anti-CD16/CD32 mouse Fc block (BD Biosciences), followed by staining for 30 min with antibodies against CD105, CD45, and CD31 (all from eBioscience) or appropriate isotype control antibodies. After washing twice, cells were subjected to FACS and $CD105^+/CD45^-/CD31^+$ endothelial cells were collected. Retrovirus expressing polyoma middle T antigen (PyMT) was used for endothelial cell immortalization (3). For flow cytometric analysis of endothelial cells, livers from E18.5 embryos (wild-type or Abl^{ECKO}; $Arg^{-/-}$) were similarly digested to a single-cell suspension, then labeled with antibodies against CD31, CD45, and Tie2 (CD202b; eBioscience) or appropriate isotype controls. Expression of each marker was evaluated by flow cytometry, and Tie2 receptor levels were examined in $CD31^+/CD45^-$ endothelial cells using FlowJo software (TreeStar Inc.). Endothelial cells were similarly isolated from hearts and livers from adult control and Abl^{ECKO}; $Arg^{+/-}$ mice, along with $CD105^-/CD45^-/CD31^-$ nonendothelial/nonhematopoietic cells. Cells were used directly for RNA isolation without culturing. Oligo $(dT)_{12–18}$-primed cDNAs were used for PCR with the following primers—Abl Flox/Δ (forward): 5′-GCC CTG GCC AGA GAT CCA TC-3′, (reverse): 5′-TCC CTC AGG TAG TCC AGC AGG-3′; Abl exon 5 (forward): 5′-GTA CGT GTC CTC CGA GAG CC-3′, (reverse): 5′-CCT TCA GGA ACT CCT CCA CC-3′; Cre (forward): 5′-CGA TGC AAC GAG TGA TGA GG-3′, (reverse): 5′-CGC ATA ACC AGT GAA ACA GC-3′; β2M (forward): 5′-ACC GGC CTG TAT GCT ATC CAG AAA-3′, (reverse): 5′-GGT GAA TTC AGT GTG AGC CAG GAT-3′. The Abl Flox/Δ primers bind to sites within *abl* exons 4 and 6, respectively; the unrecombined abl^{flox} allele yields a 500-bp PCR product, whereas a recombined abl^{Δ} allele (lacking exon 5) yields a PCR product of ∼200 bp (4).

Flow Cytometry Analysis of Fetal Liver Cells. Livers were isolated from E15.5 wild-type and Abl^{ECKO}; $Arg^{-/-}$ embryos. Livers were maintained in Hank's Balanced Salt Solution without calcium or magnesium, supplemented with 10% (vol/vol) heat-inactivated FBS and 2 mM EDTA, and were dissociated by gentle trituration. The resulting cell suspension was filtered through 70-μm and 40-μm cell strainers. Approximately 10^6 cells were used for surface staining of hematopoietic markers. Cells were first incubated with anti-CD16/CD32 mouse Fc block (BD Biosciences), followed by staining with antibodies against Kit and hematopoietic lineage markers (TER-119, GR1, B220, CD3, CD4, and CD8a) or erythroid markers (CD71 and TER-119) or appropriate isotype controls (all from eBioscience). After washing, cells were analyzed by flow cytometry and expression of cell surface markers was evaluated using FlowJo software (TreeStar Inc.).

Histological Analysis and Immunohistochemistry. Freshly dissected mouse organs were imaged using a Zeiss Lumar.V12 stereoscope. For routine histology, mouse tissue samples were fixed in 4% (wt/vol) paraformaldehyde and embedded in paraffin; 5-μm sections were used for H&E, Masson trichrome, and Prussian blue staining, following standard protocols. Images were acquired using a Zeiss Axio Imager and MetaMorph software. For FITC–wheat germ agglutinin (WGA) staining, sections were dewaxed and rehydrated, followed by proteinase K treatment (100 μg/mL, 10 min at room temperature). Slides were washed with PBS, then incubated with FITC-WGA (Sigma; 10 μg/mL, 2 h at room temperature). For immunohistochemical analysis, tissue samples were infiltrated with 30% (wt/vol) sucrose (in PBS), then fresh-frozen in tissue-freezing medium (Tissue-Tek O.C.T.; Sakura Finetek); 10-μm sections were fixed/permeabilized in ice-cold acetone, blocked in 5% (vol/vol) normal goat serum, and stained overnight at 4 °C with the indicated antibodies. Sections were then stained with Alexa Fluor-conjugated secondary antibodies

(Invitrogen) and counterstained with Hoechst 33342 (0.5 μg/mL). Images were acquired using a Zeiss Axiovert 200M fluorescence microscope and AxioVision software.

Viral Transduction. pLNCX vector and pLNCX/hTie2 retroviral constructs (kindly provided by Christopher Kontos, Duke University) were transfected into 293T cells, along with pCL10A1 packaging vector, using FuGENE6 reagent (Promega). Retroviral supernatants were collected and filtered 48 h post transfection. HUVECs were incubated 16–24 h with retroviral medium in the presence of 6 μg/mL Polybrene. Cells were cultured at least 2 d in 400 μg/mL geneticin selection medium or sorted for Tie2 overexpression by FACS (mouse anti-hTie2 antibody; BioLegend) before miRNA lentiviral infection. Lentiviral miRNA-mediated knockdown of *Abl*/*Arg* in HUVECs was conducted as described previously (5, 6). miRNA targeting sequences were as follows: control miRNA (GGTGTATGGGCTACTATAGAA); *Abl* miRNA (GGTGTATGAGCTGCTAGAGAA); *Arg* miRNA #1 (CCTTATCTCACCCACTCTGAA); *Arg* miRNA #2 (AGGTACTAAAGTGGCTCTGAG). HUVECs were lysed for Western blotting or used for RNA isolation 96 h post miRNA infection. In vitro Cre-mediated *Abl* deletion was performed using adenovirus expressing Cre recombinase (Ad5CMVCre-eGFP and Ad5CMV-eGFP control, obtained from the University of Iowa Gene Transfer Vector Core). Primary liver endothelial cells from $Abl^{flox/flox}$; $Arg^{+/+}$; *Tie2-Cre*$^{-/-}$ mice were incubated with adenovirus for 8 h at a multiplicity of infection of 200. Lentiviral shRNA transduction was used for *Arg* knockdown in primary mouse endothelial cells. Lentiviral shRNA plasmid [pLKO.1 vector; the RNAi Consortium (7)] targeting murine *Arg* was obtained from Open Biosystems (Thermo Scientific), and control (nonspecific) shRNA oligos were cloned into pLKO.1 vector. shRNA sequences (antisense) were as follows: control shRNA (TCGTAAGCCAGATAGTCATGC); *Arg* shRNA (TTGAGATAGGTCAATACCTGG). Transduced cells were selected in 1 μg/mL puromycin for at least 2 d.

Lysis and Western Blotting. Cultured cells were lysed in radioimmunoprecipitation assay (RIPA) buffer with protease/phosphatase inhibitors. Alternatively, freshly dissected mouse tissues were flash-frozen in liquid nitrogen, then homogenized in RIPA buffer containing protease/phosphatase inhibitors. Cell/tissue debris was removed by microcentrifugation, and protein concentrations were quantified. Equal amounts of protein were separated by SDS/PAGE and transferred to nitrocellulose membranes. Membranes were probed with the indicated antibodies.

Real-Time RT-PCR Array. RNA was isolated from control or *Abl*/*Arg*-knockdown HUVECs 120 h post miRNA infection, using a Qiagen RNeasy kit. One microgram of each RNA was used for cDNA synthesis, using an RT^2 First Strand cDNA kit (SABiosciences). Gene expression was evaluated using the SABiosciences Human Endothelial Cell Biology Real-Time RT-PCR Array, according to the manufacturer's protocol.

Real-Time RT-PCR Analysis. RNA was isolated from HUVECs using an illustra RNAspin Mini RNA isolation kit (GE Healthcare), and cDNA was synthesized using $Oligo(dT)_{12–18}$ primer and M-MLV reverse transcriptase (Invitrogen). Real-time PCR was performed using iQ SYBR Green Supermix (Bio-Rad). Primers used were as follows—*Tie2*/*Tek* (forward): 5′-GGG CTA CAG ACT GGA GAA GC-3′, (reverse): 5′-TGT CAA GGG TCT CCC ATG CC-3′; *Tie1* (forward): 5′-ACC CTG GTG TGC ATC CGC AG-3′, (reverse): 5′-GTG ATG TCC TCC CAC TCT AGC-3′; *Angpt1* (forward): 5′-ACT GGG AAG GGA ACC GAG CC-3′, (reverse): 5′-TGG AGG GGC CAC AAG CAT CAA-3′; *Angpt2* (forward): 5′-GAC ACA CCA CGA ATG GCA TC-3′, (reverse): 5′-CTG AAG GGT TAC CAA ATC CC-3′; *RPLP0* (forward): 5′-GGA CAT GTT GCT GGC CAA TAA-3′, (reverse): 5′-GGG CCC GAG ACC AGT GTT-3′. Analysis was performed using a Bio-Rad CFX384 real-time machine and CFX Manager software. PCR assays were performed in triplicate. Expression levels of each gene were normalized to the expression of the *RPLP0* ribosomal protein housekeeping control gene.

1. Shao R, et al. (2004) Acquired expression of periostin by human breast cancers promotes tumor angiogenesis through up-regulation of vascular endothelial growth factor receptor 2 expression. *Mol Cell Biol* 24(9):3992–4003.
2. Peters KG, et al. (1998) Expression of Tie2/Tek in breast tumour vasculature provides a new marker for evaluation of tumour angiogenesis. *Br J Cancer* 77(1): 51–56.
3. Carmeliet P, et al. (1999) Targeted deficiency or cytosolic truncation of the VE-cadherin gene in mice impairs VEGF-mediated endothelial survival and angiogenesis. *Cell* 98(2): 147–157.
4. Moresco EM, Donaldson S, Williamson A, Koleske AJ (2005) Integrin-mediated dendrite branch maintenance requires Abelson (Abl) family kinases. *J Neurosci* 25(26):6105–6118.
5. Li R, Pendergast AM (2011) Arg kinase regulates epithelial cell polarity by targeting β1-integrin and small GTPase pathways. *Curr Biol* 21(18):1534–1542.
6. Smith-Pearson PS, Greuber EK, Yogalingam G, Pendergast AM (2010) Abl kinases are required for invadopodia formation and chemokine-induced invasion. *J Biol Chem* 285(51):40201–40211.
7. Moffat J, et al. (2006) A lentiviral RNAi library for human and mouse genes applied to an arrayed viral high-content screen. *Cell* 124(6):1283–1298.

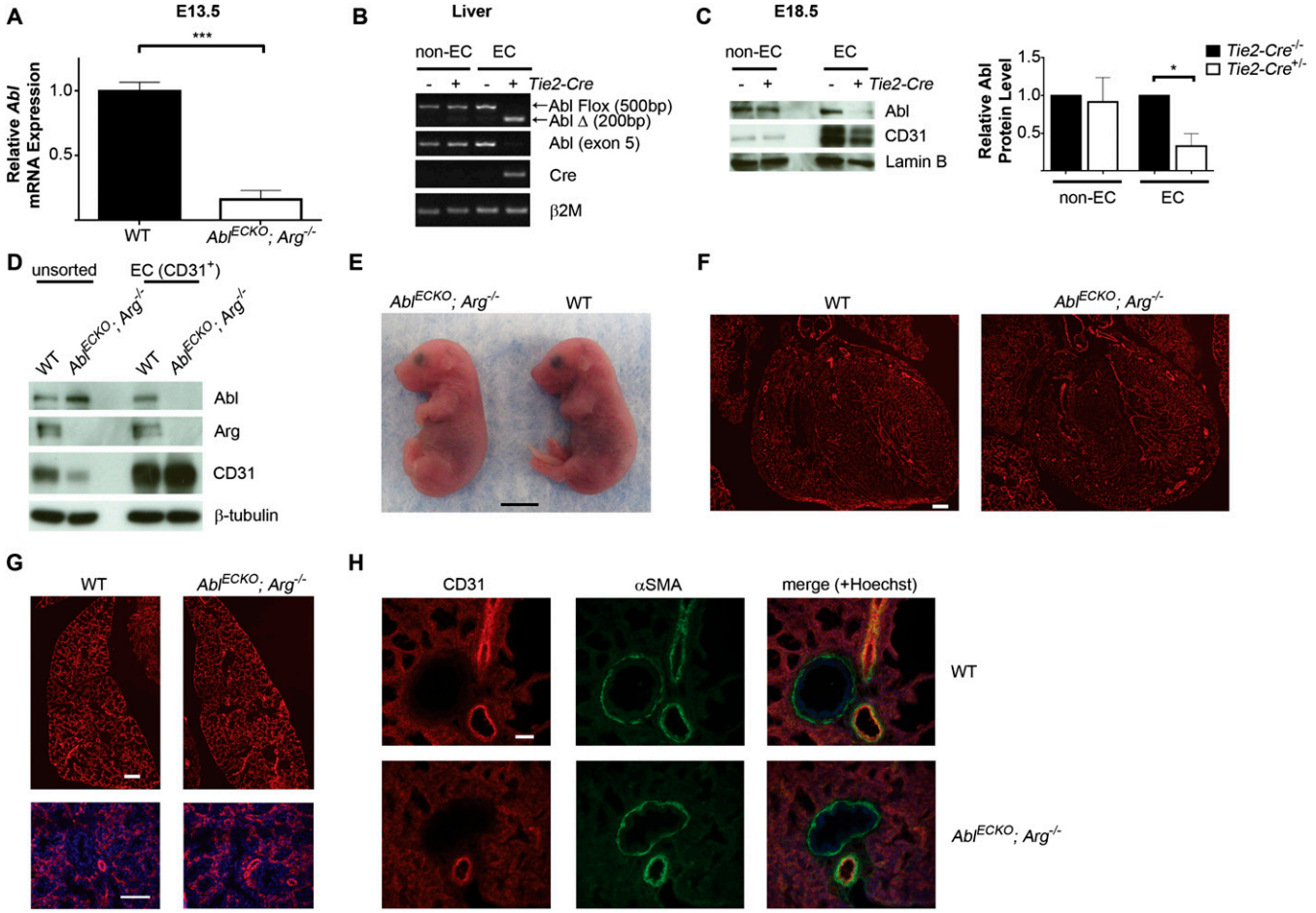

Fig. S1. Characterization of Abl^{ECKO}; $Arg^{-/-}$ embryos. (*A*) Assessment of *Abl* knockdown levels in Abl^{ECKO}; $Arg^{-/-}$ embryos. Endothelial cells ($CD105^+/CD45^-/CD31^+$) were isolated from E13.5 $Abl^{flox/flox}$; $Arg^{+/+}$; *Tie2-Cre*$^{-/-}$ (wild-type, WT) and Abl^{ECKO}; $Arg^{-/-}$ (mutant) embryos. *Abl* mRNA expression was assessed by real-time RT-PCR. Data are shown as means ± SD, n = five to six embryos per genotype. (*B*) Endothelial-specific *Abl* inactivation in livers from Abl^{ECKO}; $Arg^{+/-}$ adult mice. RNA was isolated from endothelial (EC; $CD105^+/CD45^-/CD31^+$) and nonhematopoietic/nonendothelial (non-EC; $CD105^-/CD45^-/CD31^-$) liver cell populations from Abl^{ECKO}; $Arg^{+/-}$ (+ *Tie2-Cre*) and $Arg^{+/-}$ control (– *Tie2-Cre*) mice, and Cre-mediated recombination of *abl* exon 5 was assessed by RT-PCR. Deletion of *abl* exon 5 was observed only in endothelial cells (200-bp band in top panel vs. 500-bp band in nonrecombined allele). (*C*) Abl protein depletion specifically in endothelial (EC; $CD105^+/CD45^-/CD31^+$) cells, rather than nonhematopoietic/nonendothelial (non-EC; $CD105^-/CD45^-/CD31^-$) cells, from E18.5 $Abl^{flox/flox}$; *Tie2-Cre*$^{-/-}$ and $Abl^{flox/flox}$; *Tie2-Cre*$^{+/-}$ embryos, quantified at *Right* (means ± SD, n = 3). (*D*) Analysis of Abl and Arg protein depletion in PyMT-immortalized cells from WT and Abl^{ECKO}; $Arg^{-/-}$ embryos, either before (unsorted) or after sorting for $CD31^+$ endothelial cells (EC). (*E*) Image of E18.5 WT and Abl^{ECKO}; $Arg^{-/-}$ embryos. Scale bar: 1 mm. (*F*) CD31 staining of heart sections from E18.5 WT and Abl^{ECKO}; $Arg^{-/-}$ embryos. Scale bar, 100 μm. (*G*) CD31 staining (red) of lung sections from E18.5 WT and Abl^{ECKO}; $Arg^{-/-}$ embryos. Scale bars, 100 μm (*Upper*) and 50 μm (*Lower*). (*H*) Costaining of lung sections from E18.5 WT and Abl^{ECKO}; $Arg^{-/-}$ embryos for CD31 (red) and α-smooth muscle actin (αSMA, green). Scale bar, 20 μm. *$P < 0.05$; ***$P < 0.001$.

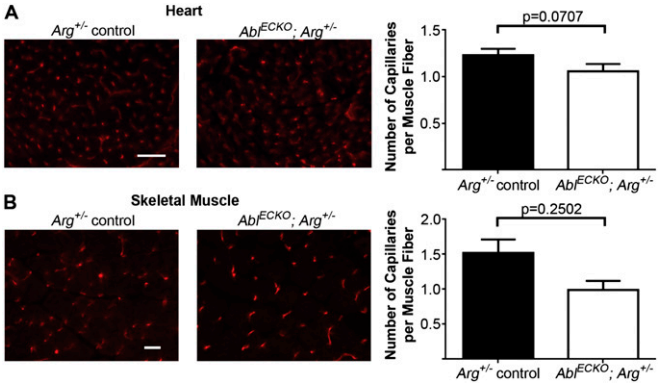

Fig. S2. Normal capillary density in heart and skeletal muscle of Abl^{ECKO}; $Arg^{+/-}$ adult mice. (*A*) CD31 staining of heart cross-sections from 8-wk-old $Arg^{+/-}$ control ($Abl^{flox/flox}$; $Arg^{+/-}$; $Tie2\text{-}Cre^{-/-}$) and Abl^{ECKO}; $Arg^{+/-}$ mice, revealing comparable capillary density, quantified at *Right* (means ± SD, *n* = three mice per genotype). (*B*) CD31 staining of tibialis anterior muscle cross-sections from 8-wk-old $Arg^{+/-}$ control and Abl^{ECKO}; $Arg^{+/-}$ mice. No significant difference was observed, although a trend toward decreased capillary density was noted in Abl^{ECKO}; $Arg^{+/-}$ mice (*Right*; means ± SD, *n* = three mice per genotype). Scale bars in *A* and *B*: 20 μm.

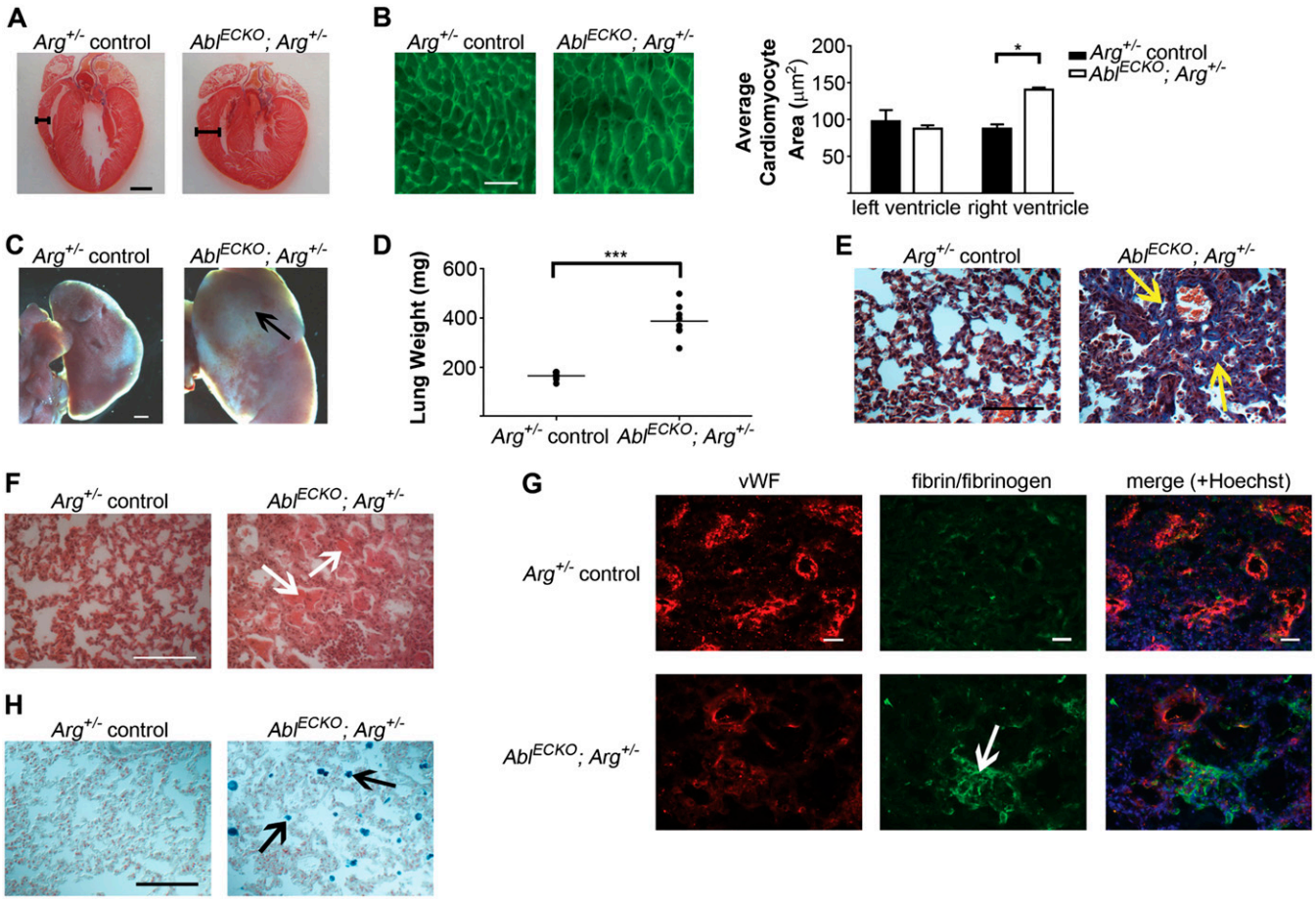

Fig. S3. Right ventricular hypertrophy and pulmonary fibrosis in Abl^{ECKO}; $Arg^{+/-}$ mice. (*A*) Trichrome-stained heart sections from 8-wk-old $Arg^{+/-}$ control ($Abl^{flox/flox}$; $Arg^{+/-}$; $Tie2\text{-}Cre^{-/-}$) and Abl^{ECKO}; $Arg^{+/-}$ mice, displaying increased right ventricle wall thickness in Abl^{ECKO}; $Arg^{+/-}$ heart (brackets). Scale bar, 1 mm. (*B*) FITC-WGA staining of right ventricle cross-sections, demonstrating an increased cardiomyocyte cross-sectional area in Abl^{ECKO}; $Arg^{+/-}$ right ventricle, quantified at *Right* (means ± SD, *n* = three mice per genotype). Scale bar, 20 μm. (*C*) Stereoscopic image of lungs from 8-wk-old $Arg^{+/-}$ control and Abl^{ECKO}; $Arg^{+/-}$ mice. Abl^{ECKO}; $Arg^{+/-}$ lungs displayed regions of apparent fibrosis (arrow). Scale bar, 1 mm. (*D*) Quantification of weights of lungs from $Arg^{+/-}$ control and Abl^{ECKO}; $Arg^{+/-}$ mice (lines indicate mean values, *n* = eight mice per genotype). (*E*) Trichrome staining, displaying collagen deposition in Abl^{ECKO}; $Arg^{+/-}$ lung (blue staining; arrows). Scale bar, 100 μm. (*F*) H&E staining of lung sections, demonstrating fibrin deposition in airways of Abl^{ECKO}; $Arg^{+/-}$ lung (arrows). Scale bar, 100 μm. (*G*) Costaining of lung sections for vWF (endothelial cell marker, red) and fibrin/fibrinogen (green). Loss of vessel density, as well as fibrin deposition (arrow), was observed in Abl^{ECKO}; $Arg^{+/-}$ lung. Scale bars, 20 μm. (*H*) Prussian blue (iron) staining, showing accumulation of hemosiderin-laden macrophages (blue staining; arrows) in Abl^{ECKO}; $Arg^{+/-}$ lung. Scale bar, 100 μm. $^{*}P < 0.05$; $^{***}P < 0.001$.

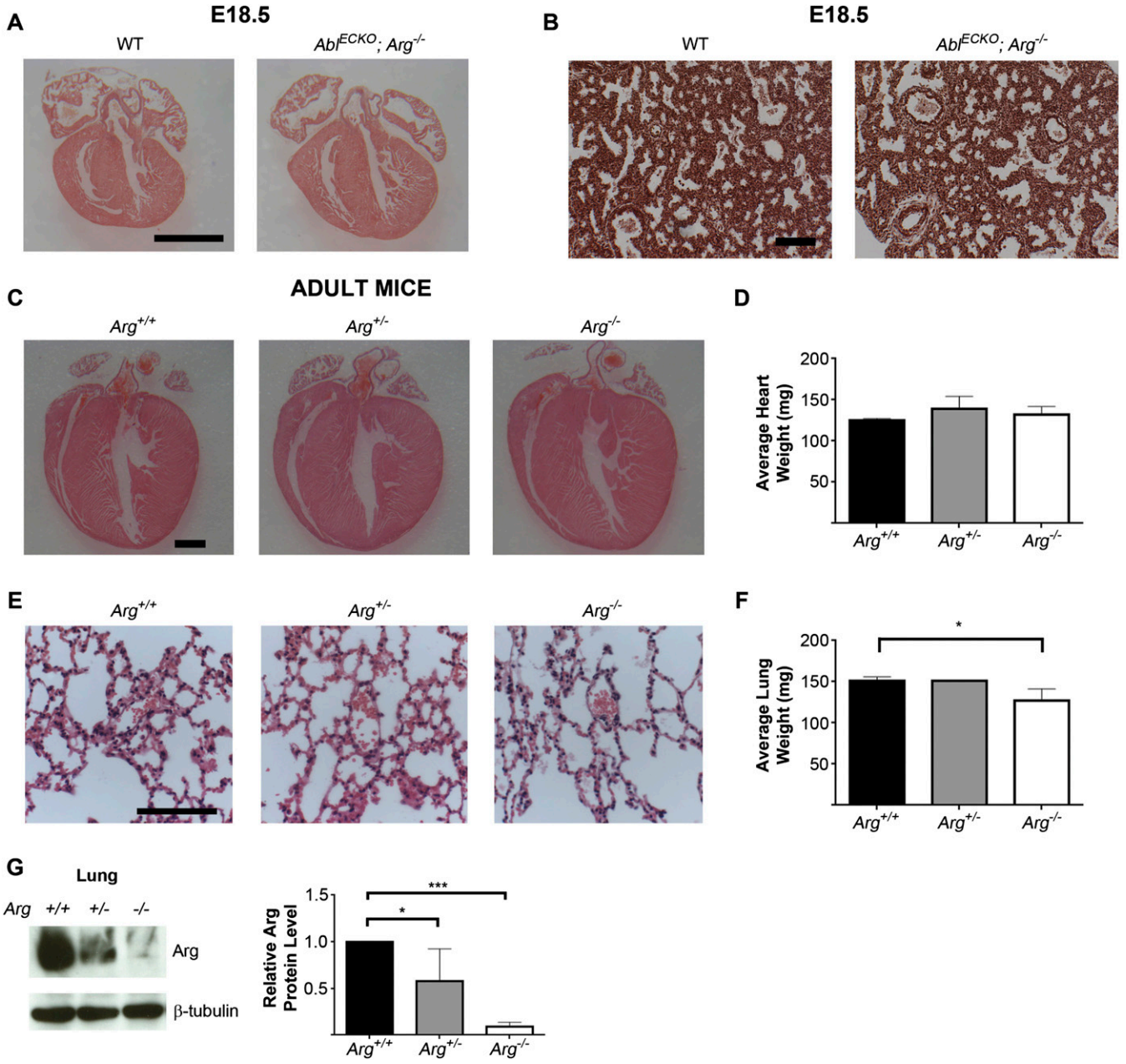

Fig. S4. Lack of cardiac hypertrophy and pulmonary fibrosis in Abl^{ECKO}; $Arg^{-/-}$ embryos and $Arg^{-/-}$ adult mice. (*A*) H&E-stained heart sections from E18.5 $Abl^{flox/flox}$; $Arg^{+/+}$; *Tie2-Cre*$^{-/-}$ (wild-type, WT) and Abl^{ECKO}; $Arg^{-/-}$ embryos. Scale bar, 1 mm. (*B*) H&E-stained lung sections from E18.5 wild-type (WT) and Abl^{ECKO}; $Arg^{-/-}$ embryos. Scale bar, 100 μm. (*C*) H&E-stained heart sections from 8-wk-old $Arg^{+/+}$ ($Abl^{flox/flox}$; $Arg^{+/+}$; *Tie2-Cre*$^{-/-}$), $Arg^{+/-}$ ($Abl^{flox/flox}$; $Arg^{+/-}$; *Tie2-Cre*$^{-/-}$), and $Arg^{-/-}$ ($Abl^{flox/flox}$; $Arg^{-/-}$; *Tie2-Cre*$^{-/-}$) mice. Scale bar, 1 mm. (*D*) Quantification of weights of hearts from $Arg^{+/+}$, $Arg^{+/-}$, and $Arg^{-/-}$ adult mice (means ± SD, n = three mice per genotype). (*E*) H&E-stained lung sections from 8-wk-old $Arg^{+/+}$, $Arg^{+/-}$, and $Arg^{-/-}$ mice. Scale bar, 100 μm. (*F*) Quantification of weights of lungs from $Arg^{+/+}$, $Arg^{+/-}$, and $Arg^{-/-}$ adult mice (means ± SD, n = three mice per genotype). A mild reduction in average lung weight was noted in $Arg^{-/-}$ mice, likely resulting from the slightly lower body weights of these animals (body weights ~85–90% of wild-type littermates). (*G*) Assessment of Arg protein levels in lung homogenates from $Arg^{+/+}$, $Arg^{+/-}$, and $Arg^{-/-}$ adult mice, quantified at *Right* (means ± SD, n = three mice per genotype). $^{*}P < 0.05$; $^{***}P < 0.01$.

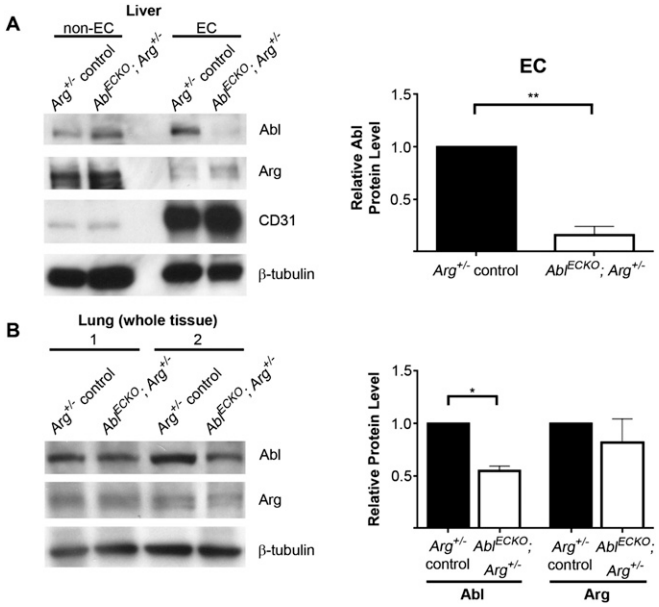

Fig. S5. Characterization of Abl and Arg Protein Levels in *Abl*^{ECKO}*; Arg*$^{+/-}$ Adult Mice. (*A*) Analysis of Abl and Arg protein levels in endothelial (EC; CD105^{+}/CD45^{-}/CD31^{+}) and nonhematopoietic/nonendothelial (non-EC; CD105^{-}/CD45^{-}/CD31^{-}) liver cell populations from *Arg*$^{+/-}$ control (*Abl*$^{flox/flox}$*; Arg*$^{+/-}$*; Tie2-Cre*$^{-/-}$) and *Abl*^{ECKO}*; Arg*$^{+/-}$ adult mice, demonstrating endothelial cell-specific Abl depletion in *Abl*^{ECKO}*; Arg*$^{+/-}$ mice, quantified in right panel (means $^{+/-}$ SD, $n = 3$). (*B*) Analysis of Abl and Arg protein levels in whole tissue homogenates from lungs of two pairs of *Arg*$^{+/-}$ control and *Abl*^{ECKO}*; Arg*$^{+/-}$ adult mice, quantified in right panel (means $^{+/-}$ SD, $n = 3$). While Arg protein levels were comparable in whole tissue homogenates from lungs of *Arg*$^{+/-}$ control and *Abl*^{ECKO}*; Arg*$^{+/-}$ mice, reduced Abl levels were observed in *Abl*^{ECKO}*; Arg*$^{+/-}$ lungs, likely as a result of the high vascular content of this tissue. *$P < 0.05$; **$P < 0.01$.

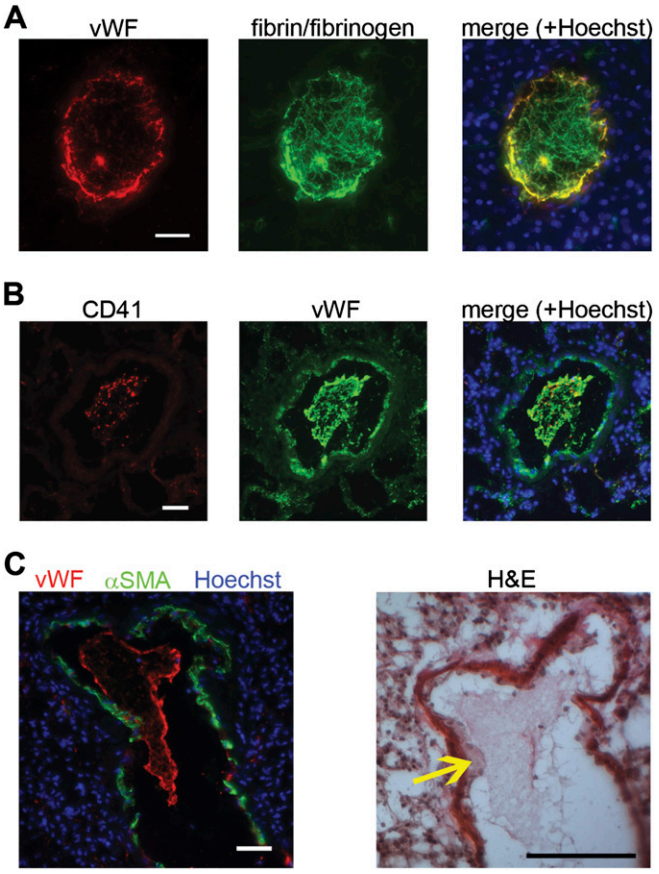

Fig. S6. Vascular occlusions in Abl^{ECKO}; $Arg^{+/-}$ Mice. (*A*) Costaining of Abl^{ECKO}; $Arg^{+/-}$ liver sections for vWF (red) and fibrin/fibrinogen (green). (*B*) Costaining of Abl^{ECKO}; $Arg^{+/-}$ lung sections for CD41 (platelet marker, red) and vWF (green). Scale bars in *A* and *B*: 20 μm. (*C, Left*) Costaining of Abl^{ECKO}; $Arg^{+/-}$ lung section for vWF (red) and αSMA (green). Scale bar, 20 μm. (*Right*) H&E staining of Abl^{ECKO}; $Arg^{+/-}$ lung section, demonstrating abnormal endothelial morphology at the site of lung thrombus (arrow). Scale bar, 100 μm.

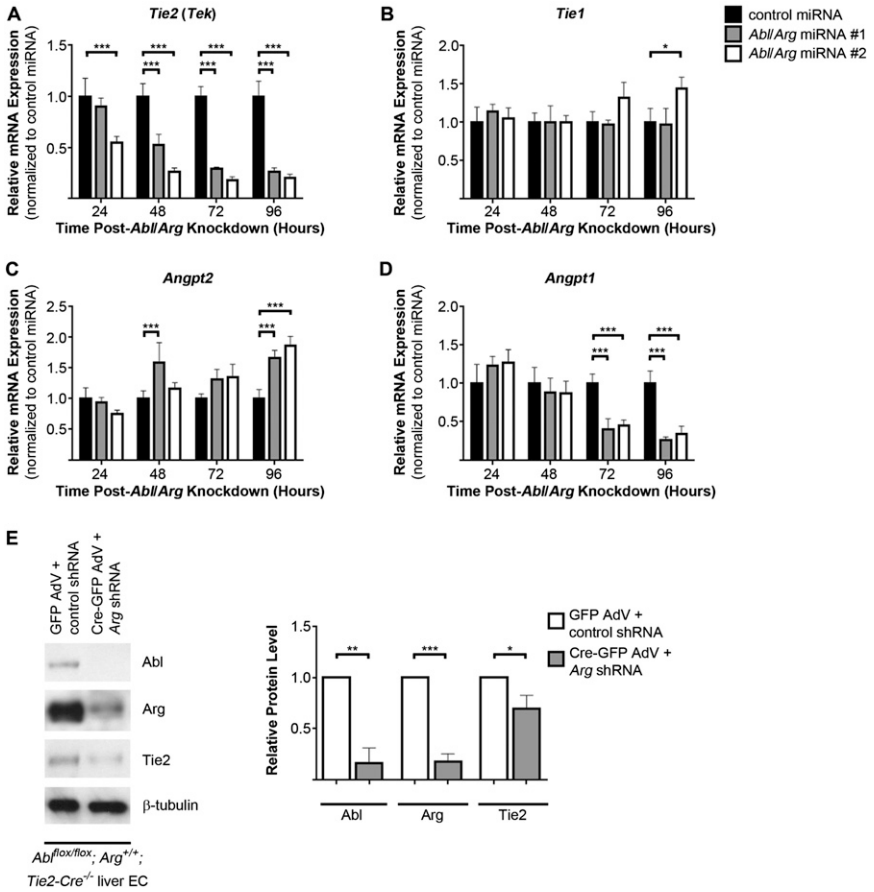

Fig. S7. Altered angiopoietin/Tie2 levels following *Abl/Arg* knockdown. (*A–D*) Real-time RT-PCR analysis of expression of (*A*) *Tie2* (*Tek*), (*B*) *Tie1*, (*C*) *Angpt2*, and (*D*) *Angpt1* in HUVECs 24–96 h following infection with either control or *Abl/Arg* miRNA lentiviruses. Fold changes in gene expression are shown relative to levels in cells expressing control miRNA. Data are presented as means ± SD ($n = 3$). (*E*) Analysis of levels of Tie2 protein in primary endothelial cells (EC) isolated from livers of $Abl^{flox/flox}$; $Arg^{+/+}$; $Tie2\text{-}Cre^{-/-}$ adult mice, following in vitro Abl/Arg depletion. Primary liver endothelial cells were infected with either GFP or Cre-GFP–expressing adenoviruses (AdV), followed by lentiviral transduction of either control or *Arg* shRNAs. Abl, Arg, and Tie2 protein levels (normalized to β-tubulin) are quantified at *Right*, relative to levels in control knockdown cells (means ± SD, $n = 3$). *$P < 0.05$; **$P < 0.01$; ***$P < 0.001$.

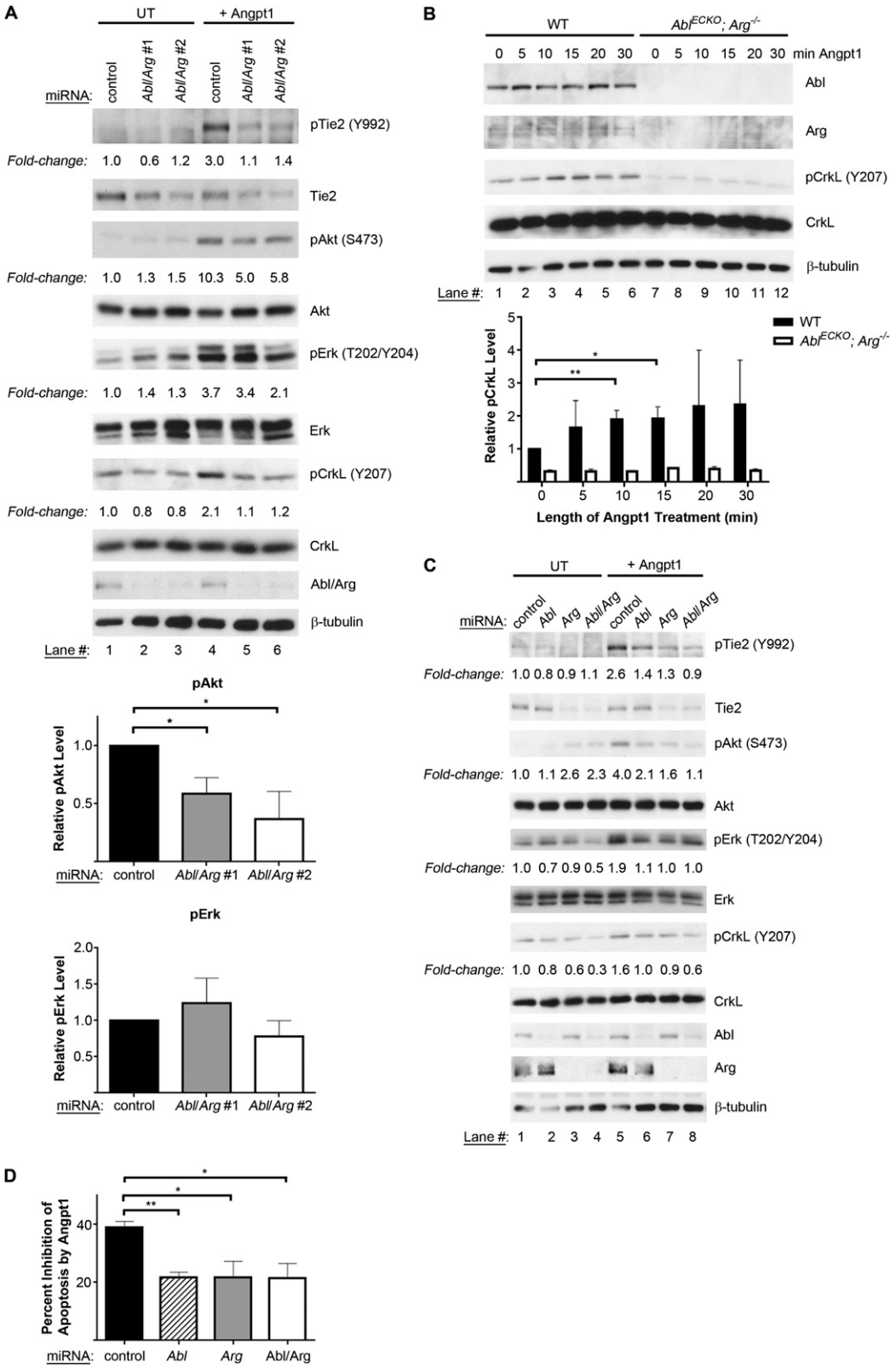

Fig. S8. Diminished angiopoietin-1–mediated signaling and survival following loss of Abl/Arg kinases. (*A*) Assessment of Angpt1-mediated activation of intracellular signaling pathways in immortalized HMVECs infected with control or *Abl/Arg* miRNA lentiviruses, quantified in bottom panels. Cells were serum starved for 6 h, then left unstimulated (UT) or treated with Angpt1 (200 ng/mL, 15 min). pAkt and pErk levels (normalized to total Akt and Erk protein) are shown as means ± SD, relative to levels in Angpt1-stimulated control miRNA-expressing cells ($n = 3$). (*B*) Assessment of the time course of Angpt1-mediated activation of Abl kinases, as determined by phospho-CrkL(Y207) levels, in PyMT-immortalized endothelial cell lines from $Abl^{flox/flox}$; $Arg^{+/+}$; *Tie2-Cre*$^{-/-}$ (wild-type, WT) and Abl^{ECKO}; $Arg^{-/-}$ embryos. (*Lower*) Fold changes in pCrkL levels (normalized to total CrkL protein) are quantified (means ± SD, $n = 3$). Angpt1

Legend continued on following page

treatment increased pCrkL levels in WT, but not *Abl*^{ECKO}; *Arg*$^{-/-}$, endothelial cells. (*C*) Assessment of Angpt1-mediated activation of intracellular signaling pathways in HUVECs expressing control miRNA, individual *Abl* or *Arg* miRNAs, or dual *Abl*/*Arg* miRNA. Fold changes in pathway activation (normalized to total protein levels) are shown, expressed relative to unstimulated (UT) control miRNA-expressing cells. (*D*) Analysis of levels of apoptosis in HUVECs after 24-h serum starvation in the presence of Angpt1 (200 ng/mL) following either *Abl* or *Arg* individual knockdown or dual knockdown of both *Abl*/*Arg* kinases. Values are expressed as percent inhibition of apoptosis by Angpt1 relative to serum-starved (nonsupplemented) cells. Data are presented as means ± SEM ($n = 3$). *$P < 0.05$; **$P < 0.01$.

Table S1. No differences in hematopoietic progenitors in *Abl*^{ECKO}; *Arg*$^{-/-}$ embryos

Cell marker	WT, %	*Abl*^{ECKO}; *Arg*$^{-/-}$, %
TER-119$^+$	80.54 ± 2.58	81.07 ± 4.15
CD71$^+$	92.48 ± 2.50	92.93 ± 3.35
TER-119$^+$/CD71$^+$	79.34 ± 3.07	80.23 ± 4.61
Lin$^-$	20.70 ± 1.98	20.80 ± 2.92
Kit$^+$	14.40 ± 2.02	14.13 ± 2.58
Lin$^-$/Kit$^+$	12.66 ± 1.04	12.60 ± 1.70

Fetal liver cells were isolated from E15.5 WT and *Abl*^{ECKO}; *Arg*$^{-/-}$ embryos, and their expression of various hematopoietic markers was assessed by flow cytometry. No differences in the percentages of lineage-negative (Lin$^-$)/Kit$^+$ hematopoietic progenitors or TER-119$^+$/CD71$^+$ erythroid progenitors were observed. Data are presented as means (%) ± SD (WT, n = five embryos; *Abl*^{ECKO}; *Arg*$^{-/-}$, n = three embryos).